Room temperature InGaSb quantum well microcylinder lasers at 2 μm grown monolithically on a silicon substrate

Tian Yang,[a)] Ling Lu, Min-Hsiung Shih, and J. D. O'Brien
Department of Electrical Engineering-Electrophysics, University of Southern California, 3737 Watt Way, PHE 604, Los Angeles, California 90089

Ganesh Balakrishnan and D. L. Huffaker
Center for High Technology Materials, Electrical and Computer Engineering, University of New Mexico, Albuquerque, New Mexico 87106

(Received 2 February 2007; accepted 7 August 2007; published 5 September 2007)

Fabrication of microcylinder laser cavities in III-Sb material on a silicon substrate is reported. Room temperature lasing near 2 μm wavelength under optical pumping conditions is demonstrated in the microcylinders with InGaSb quantum wells. The III-Sb material is grown monolithically on a silicon substrate. High quality epitaxy is enabled by an interfacial misfit array. © *2007 American Vacuum Society.* [DOI: 10.1116/1.2778693]

I. INTRODUCTION

Antimonide based semiconductor lasers have been developed for high performance sources in the midinfrared wavelength range. Ultralow lasing threshold has been reported for broadened-waveguide diode lasers at 2 μm with GaInAsSb quantum well (QW) active material grown on a GaSb substrate.[1] Yet microfabrication techniques for III-Sb materials are not as well developed as for III-As materials. In this article, we demonstrate the fabrication of microcylinder lasers with InGaSb QW active material and their room temperature photopumped lasing at 2.0 μm. The III-Sb material is grown monolithically on a silicon (100) substrate.

The large lattice mismatch and thermal expansion coefficient mismatch that exists between most III-V's and silicon have hindered the monolithic integration of light emitters and complementary metal-oxide semiconductor technologies. In our devices, the III-Sb nucleation and subsequent high quality bulk epitaxy are enabled by a recently reported growth mode based on an interfacial misfit (IMF) array formed at the AlSb/Si interface. The IMF eliminates strain energy immediately at the interface resulting in very low defect density ($\sim 8 \times 10^5/\mathrm{cm}^2$) and relaxed bulk material growth (98%).[2,3] Furthermore, the III-Sb material has a good thermal expansion coefficient match with the silicon substrate, unlike III-As materials.

II. FABRICATION

The epitaxial structure, shown in Fig. 1, was grown by molecular beam epitaxy on a silicon (100) substrate. Lattice mismatch and strain between the antimonide material and the silicon substrate are released by the IMF array at the interface of silicon and AlSb.[2] The epitaxial structure consists of an AlSb/GaSb superlattice followed by an $Al_{0.9}Ga_{0.1}Sb$ cladding layer (1.5 μm) and an $Al_{0.3}Ga_{0.7}Sb_{0.93}As_{0.07}$ waveguide (0.5 μm) surrounding the active region. The waveguide is lattice matched to the cladding layer. The active region includes three $In_{0.2}Ga_{0.8}Sb$ quantum wells (130 Å) separated by $Al_{0.3}Ga_{0.7}Sb_{0.93}As_{0.07}$ barriers (200 Å). A 50 nm GaSb cap layer protects the AlGaSb cladding from natural oxidation.

The device processing procedure is summarized in Fig. 2. It began with the deposition of a 0.5 μm silicon nitride layer onto the antimonide material by chemical vapor deposition (CVD) followed by spin coating six layers of polymethyl methacrylate (PMMA). 1 h baking on hot plate at 180 °C was done between each PMMA spin deposition. The total thickness of the PMMA was just over 1 μm. A thick PMMA mask was used because of the low selectivity between PMMA and silicon nitride in a later CF_4 dry etching step. The microcylinders were defined in PMMA by electron beam lithography at 30 kV and developed in MIBK:IPA =1:2. The PMMA was hardened afterwards by a blank exposure in the electron microscope. Then the microcylinder patterns were transferred into the silicon nitride by dry etching with CF_4 in an electron cyclotron resonance etcher in the reactive ion etching (RIE) mode. The etching conditions were 490 W rf power and 11 mtorr pressure. By monitoring the color change of the sample surface under illumination from the CF_4 plasma, it was ensured that silicon nitride etching was complete yet the antimonide material was not noticeably etched. CF_4 plasma changes the PMMA on silicon nitride and makes it very difficult to remove. We followed Ref. 4 to remove the PMMA using a combination of acetone rinse, acetone ultrasonic cleaning, and oxygen plasma etching in a RIE. Half of the microcylinders in silicon nitride had very clean and smooth surfaces after this step, as shown in Fig. 3. It is important in this step to choose an appropriate compromise between a long time oxygen plasma etching which more completely removes the PMMA residue and a short time oxygen plasma etching which does less harm to the materials. As shown in Fig. 3, a dark layer formed on the top of the microcylinders in silicon nitride. This dark layer comes from the reaction between oxygen plasma and silicon nitride.[5] Its thickness increases with the oxygen plasma etch-

[a)]Author to whom correspondence should be addressed; electronic mail: tianyang@deas.harvard.edu

Layer	
GaSb 0.05μm	
$Al_{0.9}Ga_{0.1}Sb$ 1.5μm	cladding
$Al_{0.3}Ga_{0.7}SbAs$ 0.5μm	waveguide
$In_{0.2}Ga_{0.8}Sb$ 0.013μm	3 quantum wells
$Al_{0.3}Ga_{0.7}SbAs$ 0.02μm	3 quantum wells
$In_{0.2}Ga_{0.8}Sb$ 0.013μm	3 quantum wells
$Al_{0.3}Ga_{0.7}SbAs$ 0.02μm	3 quantum wells
$In_{0.2}Ga_{0.8}Sb$ 0.013μm	3 quantum wells
$Al_{0.3}Ga_{0.7}SbAs$ 0.5μm	waveguide
$Al_{0.9}Ga_{0.1}Sb$ 1.5μm	cladding
GaSb 0.1μm / AlSb 0.1μm ×15	
Si substrate	

FIG. 1. Epitaxial structure of the material for microcylinder cavities.

ing time. It is also for this reason that we did not clean the sample with oxygen ashing after the development of PMMA in order not to change the properties of the silicon nitride mask before transferring the patterns into silicon nitride in CF_4 plasma. As will be discussed later in this paragraph, this oxygen plasma etching step also damages the top part of the antimonide material. For the laser cavities, the oxygen plasma RIE conditions used to remove the PMMA residue were 50 W power and 200 mtorr pressure for 15 min. Then the microcylinder patterns were transferred into the antimonide using an inductively coupled plasma (ICP) etching with BCl_3 and N_2.[6] The etching conditions in the ICP were temperature of 70 °C (the lowest possible for this ICP equipment), pressure of 2 mtorr, N_2 flow of 5 SCCM (SCCM denotes cubic centimeter per minute at STP), BCl_3 flow of 10 SCCM, power of 600 W, dc bias of 300 V, and etching time of 2.25 min. By comparing the etching results at dc

(a)

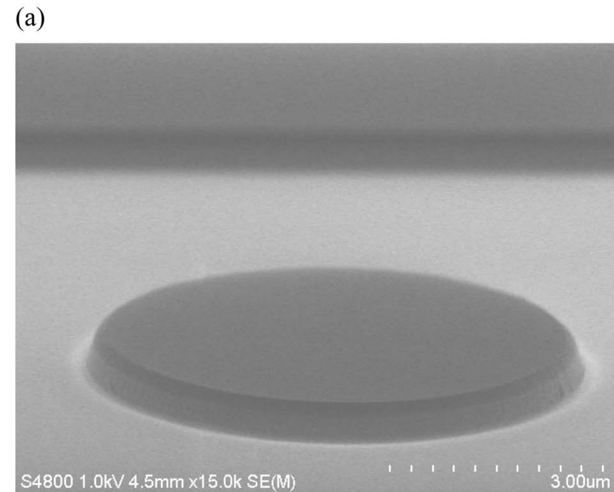

(b)

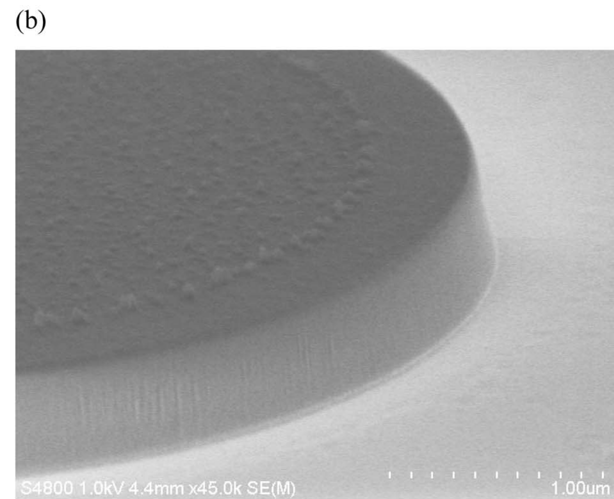

FIG. 3. Scanning electron micrographs of microcylinders in silicon nitride after removal of PMMA by acetone and oxygen plasma etching. Both cylinders in (a) and (b) were etched in oxygen plasma in a RIE at 50 W and 200 mtorr. The cylinder in (a) was etched for 60 min and the one in (b) was etched for 15 min.

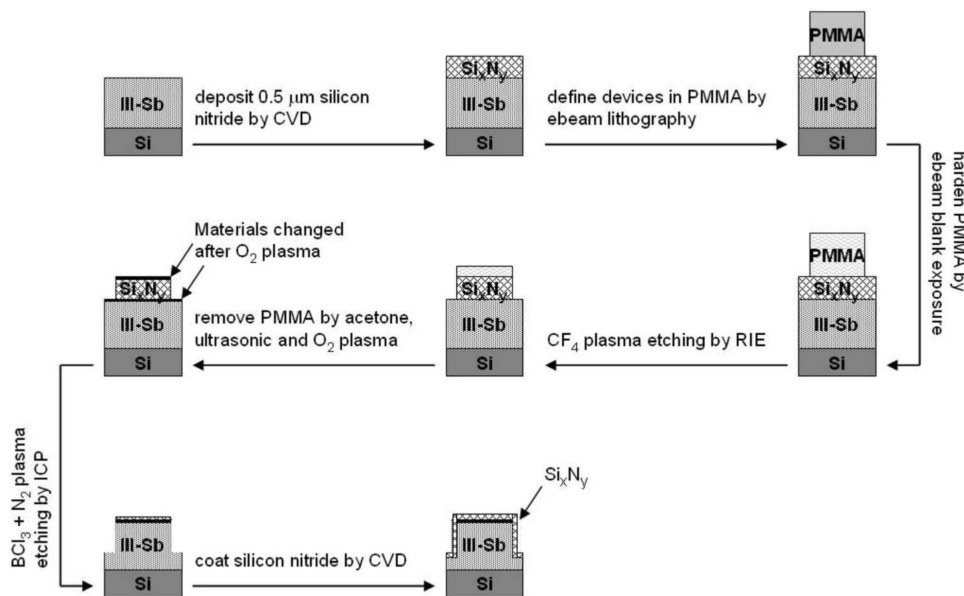

FIG. 2. Fabrication procedure.

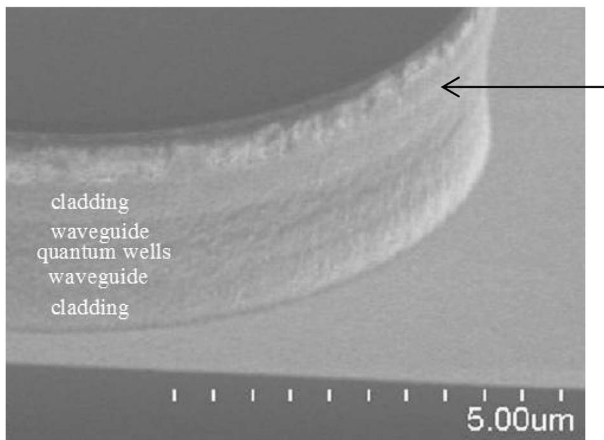

FIG. 4. Scanning electron micrograph of a microcylinder in antimonide after ICP etching. The arrow is pointing at the oxygen plasma RIE etching induced line.

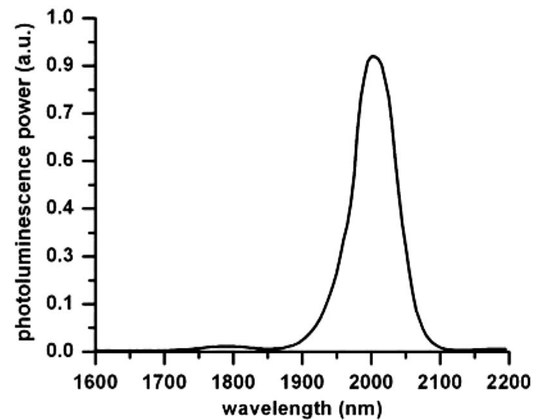

FIG. 6. Broad area photoluminescence from nonpatterned InGaSb quantum well material.

biases of 200, 300, and 400 V, we found that with higher dc bias in ICP, the sidewalls of the microcylinders in the antimonide material are straighter and smoother, while the etching selectivity of antimonide to silicon nitride is smaller. We chose the dc bias voltage of 300 V as a compromise because of the difficulty in the deposition of thick silicon nitride and PMMA masks. A scanning electron micrograph of a microcylinder after ICP etching is shown in Fig. 4. With our smooth silicon nitride masks, the sidewalls in antimonide can be improved by quite much compared to that in Fig. 4 by using a higher dc bias of 400 V. In Fig. 4, the arrow points to a line above which the sidewall had peeled and cracked. We found that the distance between this line and the top of the antimonide material increases with the time of oxygen plasma RIE etching which was done to remove the PMMA residue. This is the reason why we have chosen an oxygen plasma RIE etching time of not more than 15 min. Finally, the microcylinders were coated with a thin layer of silicon nitride in a CVD in order to protect the high aluminum con-

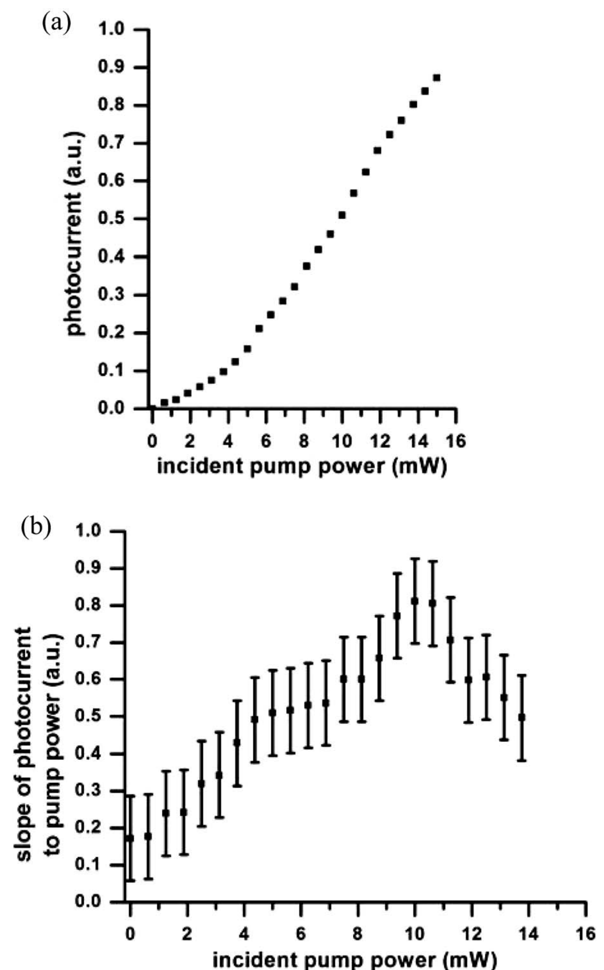

FIG. 7. (a) Photoluminescence from a 5 μm diameter microcylinder device collected by a p-i-n photodiode vs incident peak pump power at 850 nm. Pumping conditions are 24 ns pulse widths and a 12% duty cycle. (b) Photocurrent-to-incident-peak-pump-power differential slope vs incident peak pump power for the same device.

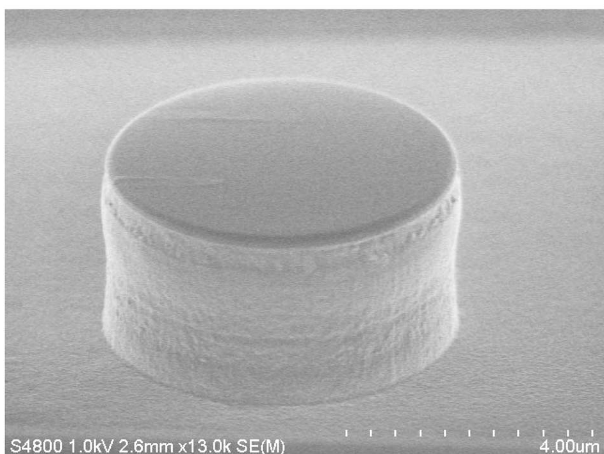

FIG. 5. Scanning electron micrograph of a microcylinder after the whole fabrication procedure.

tent sidewalls from natural oxidation. A scanning electron micrograph of a finished device is shown in Fig. 5.

III. PHOTOPUMPED LASING

Broad area photoluminescence (PL) from the nonpatterned InGaSb quantum well material was obtained by optical pumping with a mode-locked Ti:sapphire laser at 775 nm. The Ti:sapphire laser had a 200 fs pulse width and a 1 kHz repetition rate. Emission from the quantum wells was collected into an InSb detector. The broad area PL was centered around 2.0 μm and had a full width at half maximum (FWHM) of 75 nm as in Fig. 6.

The microcylinder devices were optically pumped at room temperature with a semiconductor laser diode at 850 nm. The pump beam was focused by a microscope objective to a 1–2 μm diameter pump spot at normal incidence onto the center of the microcylinder cavities. PL from the devices was collected by the same microscope objective and sent into an InGaAs p-i-n photodiode which has a response peaked at 2.2 μm and a FWHM of 1 μm. Scattered pump power was blocked by a silicon wafer and was not collected into the p-i-n diode. Details of the micro-PL experiment are similar to that in Ref. 7 except that here we were collecting quantum well emission at all wavelengths without dispersing it with a spectrometer. Photocurrent from the p-i-n diode versus incident optical pump power for a 5 μm diameter microcylinder is shown in Fig. 7(a). The pumping conditions are 24 ns pulse widths and a 12% duty cycle. Figure 7(b) shows the photocurrent-to-pump-power differential slope versus pump power. The kink at 4 mW pump power indicates the lasing threshold. This kink turn-on behavior was not observed for devices with lower fabrication quality. It can be explained by the different emission-pump dependences between spontaneous emission and lasing emission: $(\text{spontaneous emission}) \propto (\text{carrier density})^2 \propto (\text{pump power})^2$, under the assumption that surface recombination is dominant below threshold; $(\text{lasing emission}) \propto (\text{pump power above threshold})$, under the assumption that carrier density is clamped above threshold. This explanation is consistent with Fig. 7(b) that the emission-to-pump-power differential slope is linearly increasing below threshold and is constant above threshold. The claim of lasing is further supported by a simple analytical model which indicates that this turn-on behavior cannot be due to superluminescence because of the short round trip distance of the microcylinders. The step in the slope versus pump power behavior around 10 mW pump power likely indicates a hop to another lasing mode. The threshold turn-on kink point was also observed under continuous wave operation by increasing the size of the pump spot.

IV. SUMMARY

We report the fabrication of antimonide microcylinder laser cavities on a silicon substrate, and we have demonstrated room temperature lasing near 2 μm wavelength under optical pumping conditions.

ACKNOWLEDGMENTS

The authors acknowledge Stephen Farrell, Zhen Peng, and Qi Yang at the University of Southern California for their advice on fabrication.

[1]G. W. Turner, H. K. Choi, and M. J. Manfra, Appl. Phys. Lett. **72**, 876 (1998).
[2]G. Balakrishnan *et al.*, Electron. Lett. **41**, 531 (2005).
[3]G. Balakrishnan *et al.*, Electron. Lett. **42**, 350 (2006).
[4]R. Colombelli *et al.*, Nanotechnology **15**, 675 (2004).
[5]S. E. Hicks, S. K. Murad, I. Sturrock, and C. D. W. Wilkinson, Microelectron. Eng. **35**, 41 (1997).
[6]T. Maeda *et al.*, Appl. Surf. Sci. **143**, 174 (1999).
[7]T. Yang, S. Lipson, J. D. O'Brien, and D. G. Deppe, IEEE Photonics Technol. Lett. **17**, 2244 (2005).